n- to *p*-type conductivity transition and band-gap renormalization in ZnO:(Cu+Te) codoped films

Alfredo Beristain-Bautista,[1] Daniel Olguín,[2] and Sergio Jiménez-Sandoval [1,*]

[1]*Centro de Investigación y de Estudios Avanzados del I. P. N., Unidad Querétaro, Libramiento Norponiente No. 2000, Fracc. Real de Juriquilla, C. P. 76230, Querétaro, Qro., Mexico*

[2]*Centro de Investigación y de Estudios Avanzados del I. P. N., Departamento de Física, Av. Instituto Politécnico Nacional No. 2508, Col. San Pedro Zacatenco, C.P. 07360, Ciudad de México, Mexico*

The natural conductivity of as-grown ZnO is *n*-type. It has been challenging to produce stable *p*-type material, which has delayed possible technological applications. In this work, the conductivity transformation from *n*- to *p*-type ZnO films deposited by sputtering was followed as a function of copper and tellurium concentrations and of the substrate temperature during growth (room temperature, $150\,^\circ$C, $250\,^\circ$C, and $350\,^\circ$C). The nominal codopant concentrations ranged from 1 to 12 at %. For the minimum concentration, compensation effects yielded highly resistive ZnO. Nonetheless, by tailoring the concentration of Cu and Te, it was possible to vary the resistivity (10^3–$10^{-2}\,\Omega$ cm), mobility ($\sim 10^{-2}$–10° cm^2/V s), and free-hole density (10^{15}–10^{20} cm^{-3}) of *p*-type ZnO grown at $250\,^\circ$C. Besides modifying the electrical properties, codoping changed the host band structure significantly, producing a band-gap renormalization from 3.2 eV (UV) to 1.8 eV (red). This control over the band gap is advantageous for applications where controllable photon absorption or emission are sought. Experimentally, films were stable for a period of at least six months. Band-gap engineered *p*-type ZnO:(Cu+Te) films open the possibility for the fabrication of all-ZnO optoelectronic devices such as homojunction solar cells and/or light-emitting diodes.

Zinc oxide (ZnO) is an earth-abundant, low-cost, wide-band-gap semiconductor whose physical properties make it appropriate for a large variety of applications [1,2]. As in most wide-band-gap materials, *n*-type doping is easily or unintentionally achieved, while *p*-type doping has proven to be a challenging task. The reasons for this difficulty arise mainly from the following causes: (a) low solubility of dopants in the host, (b) deep impurity energy levels that do not contribute effectively to conductivity, and (c) the formation of low-energy compensating defects (such as Zn_i, V_O, complexes, and hydrogen, a common contaminant in growth chambers). Different approaches have been undertaken to overcome these difficulties, which include (i) codoping aimed to improve the solubility of shallow acceptors and reduce the defect ionization level, (ii) the theoretical and experimental search for appropriate group-I and group-V dopants, and (iii) modification of the ZnO band structure through appropriate defect bands inside the band gap [3]. The most common codoping approach has focused on improving the low solubility of nitrogen (an appropriate acceptor candidate due to its low ionization energy) in ZnO using acceptor-donor pairs (e.g., N and group-III elements) [4]. Although this route produced samples with *p*-type characteristics, some issues remain unsolved such as the position of the N and group-III levels within the band gap, and the long-term stability [3]. Yan *et al.* proposed reducing the dopants ionization energies by introducing acceptor-donor passivated impurity bands, complemented by an effective doping made by increasing the acceptor concentration [5].

Copper is a well-known *p*-type dopant in ZnO; however, it forms deep acceptors (ionization energy of $Cu_{Zn} = 0.35$ eV) that contribute to conductivity but not efficiently [6]. Through density functional theory calculations, it was shown that Cu affects the ZnO band structure in such a way that the top of the valence band shifts upwards and the bottom of the conduction band downwards, creating a reduced effective band gap [7]. In the case of tellurium, it has been reported that the incorporation of Te in the ZnO lattice may be beneficial in two ways. First, it suppresses the formation of Zn_i, a common *n*-type defect; second, in the alloy regime ZnO:Te modifies the host band structure, producing shallow acceptors [8]. When used as codopant with nitrogen, it has been reported that Te may act as a surfactant to decrease the formation energy of N_O defects, thus improving nitrogen solubility [9]. Moreover, it was observed that Te induced a small blue shift in the band gap of ZnO [10,11].

The approach followed in this work has focused on pursuing the use of alternative codopants. Cu is a well-known *p*-type dopant, which indicates that it enters as a substitutional impurity (Cu_{Zn}) rather than interstitial (Cu_i is a *n*-type dopant). The experimental work undertaken here shows that Te, when used as codopant with Cu, produces conductivity with holes as majority carriers. It is pointed out, however, that the experimental findings reveal that the formation of *p*-type material depends upon the concentration of Cu+Te and on the thermal energy supplied to the atomic species during growth, i.e., the substrate temperature. Additionally, in the alloy regime Cu and Te favorably modify the host band structure for hole-based conductivity. The deep acceptor characteristic of Cu, when single dopant, is lifted. Codoping ZnO with Cu

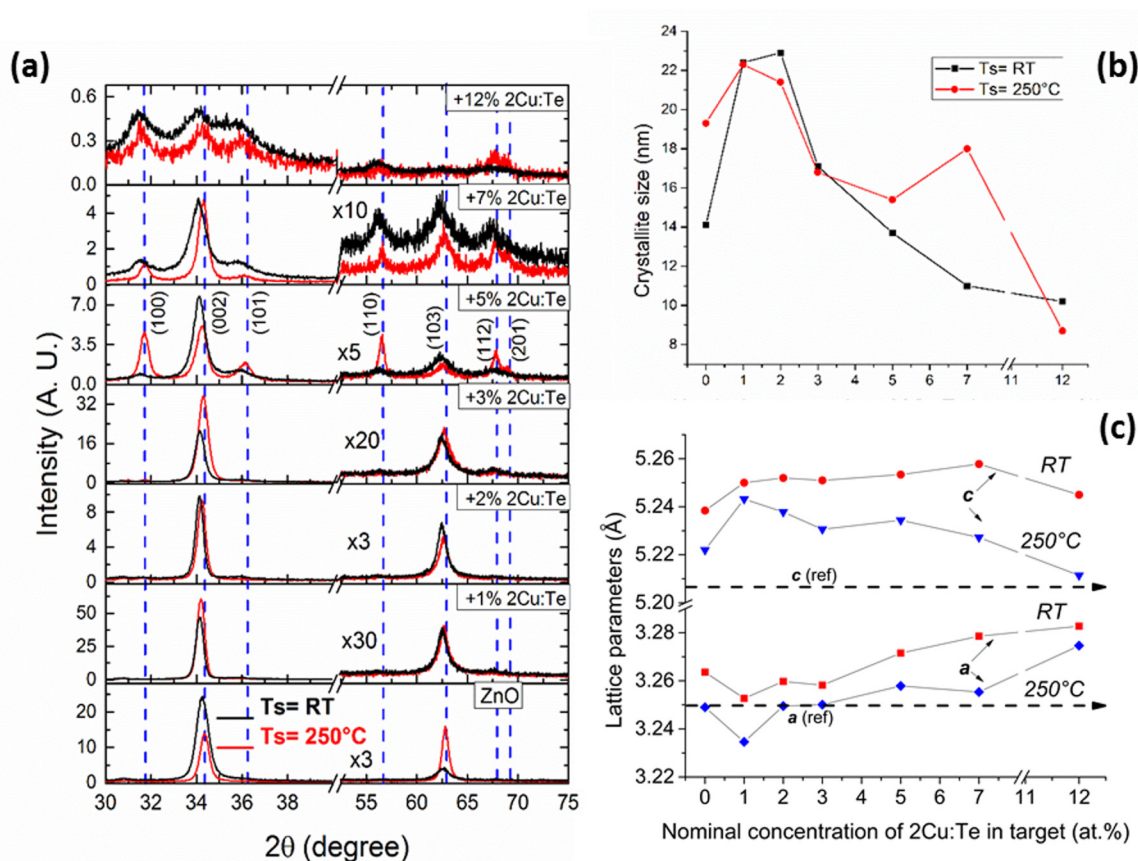*Correspondence author: sergio.jimenez@cinvestav.mx

FIG. 1. (a) X-ray diffraction patterns of films grown at RT (black) and 250 °C (red) for the indicated Cu and Te concentrations in the sputtering target. The patterns at large diffraction angles were amplified by the indicated factors. The labels of the diffraction peaks correspond to hexagonal (wurtzite) ZnO. (b) and (c) show the crystallite size and lattice parameters as a function of the dopant nominal concentration in the target, respectively. The dashed lines in (c) indicate the single-crystal values for the lattice parameters from Ref. [3].

and Te produced not only a monotonic increment in the free-hole density as their concentration rose, but also a clear *n*-to-*p* transition that passed through a highly resistive fully compensated state. It is pointed out that the conductivity transition occurred concomitantly with an important band-gap renormalization extending from the UV to the red. The electrical properties of the samples reported here were measured at least six months after their growth, which indicates good stability.

I. RESULTS AND DISCUSSION

Zinc oxide has a direct band gap (E_g) of 3.3 eV at room temperature [4]. Its thermodynamically stable phase is hexagonal (wurtzite), described by the space group $P6_3mc$. In this work, radio-frequency sputtering was used to grow ZnO:(Cu+Te) films from targets made of powdered mixtures of ZnO and appropriate amounts of Cu and Te to obtain nominal concentrations of 1, 2, 3, 5, 7, and 12 at % in an atomic ratio of 2:1, respectively. Specifically, a nominal concentration of 1% means that the target was composed of 99.00 at % ZnO, 0.66 at % Cu, and 0.33 at % Te, with analogous equivalencies for the other concentrations. The ratio 2Cu/Te was originally conceived to investigate the possible formation of micro- or nanoclusters of $Cu_{2-x}Te$, a *p*-type semimetal with a large free-hole density (typically between 10^{19} and 10^{22} cm^{-3}). Nevertheless, no experimental evidence was found consistent

with the formation of any copper telluride polytype in the samples. In spite of the actual concentration ratio of Cu and Te in the films, hereafter the dopant concentration will be generically designated by the nominal concentration in the target: (2Cu:Te).

Although the substrate temperature (T_s) varied between room temperature and 350 °C, it is clarified that the electrical characterization could be complete only for the films grown at 250 °C. For other deposition temperatures, no reliable contacts for the whole batch could be obtained, producing incomplete Hall-effect data, which are crucial for this study. Because of this and with the intention of keeping the number of figures to a reasonable number, the discussion of results is centered around the samples deposited at 250 °C. For clarity purposes, the results for other substrate temperatures are described, or shown, and properly considered in the relevant data discussion.

A. Properties and surface morphology

The x-ray diffractograms of the films showed well-defined peaks, all in agreement with those of hexagonal ZnO regardless of the amount of copper and tellurium in the target. The only sample that presented an additional reflection was the film doped with 12 at % grown at 350 °C. This diffractogram (not shown) presented a weak band at 41.7 ° identified with the (110) peak of ZnTe (PDF no. 19-1482). Figure 1(a) shows the
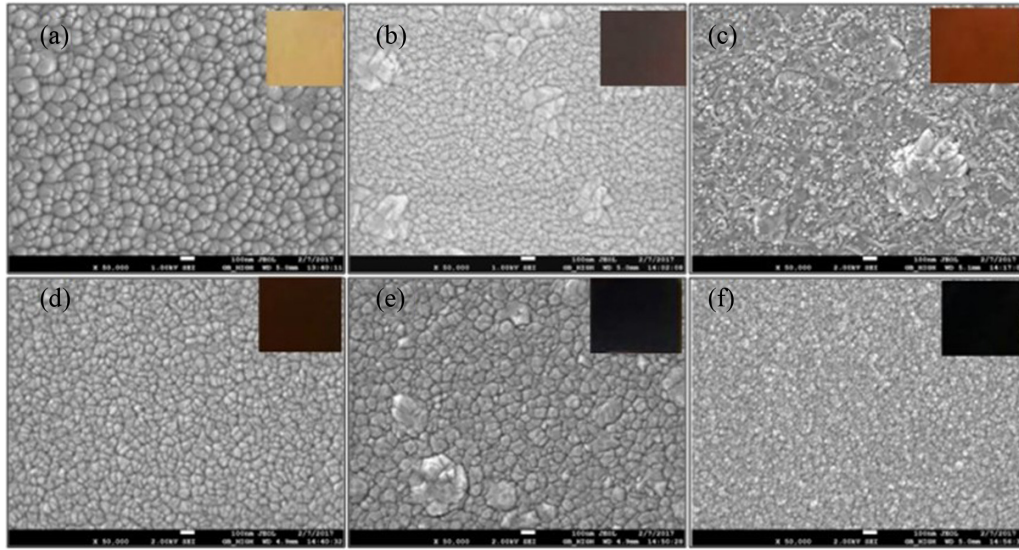
FIG. 2. Surface morphology of films grown at $250\,°C$ with (a) 1 at %, (b) 2 at %, (c) 3 at %, (d) 5 at %, (e) 7 at %, and (f) 12 at % 2Cu:Te. The scale bar corresponds to 100 nm. The insets show the appearance to the eye of each film under white-light illumination.

diffraction patterns of films grown on glass substrates at room temperature (RT) and $250\,°C$ as a function of the nominal dopant concentration in the target.

The peak positions for hexagonal (wurtzite-type) zinc oxide from the powder diffraction file (PDF no. 05-0664) are shown in dotted lines. The low-intensity peaks beyond $2\theta = 50\,°$ have been enhanced by the indicated factors. For all substrate temperatures the incorporation of 12 at % 2Cu:Te introduced substantial disorder in the lattice. The diffraction patterns of those samples were similar to the one shown at the top of Fig. 1(a). For the rest of the films in Fig. 1(a), the strong peak at $\sim 34.44\,°$ corresponds to diffraction of the ZnO (002) planes. The preferential growth along this direction gradually disappears as the dopant concentration rises. Additional diffractions, (100) and (101), appear in the patterns around the (002) peak, as well as other peaks in the region above $50\,°$. The diffraction peaks for films grown at $250\,°C$ are in better agreement with the positions of the PDF file (dashed lines) than those of the films grown at RT. Higher T_s (i.e., larger thermal energy supplied during growth) releases tensile stresses. In Fig. 1(b) are presented the values of crystallite size as a function of the dopant concentration for $T_s = $ RT and $250\,°C$. The sizes were obtained by applying the Scherrer relation to the (002) peak of each diffractogram. The crystallite size attained a maximum value (22.9 nm for 2 at % for $T_s = $ RT, and 22.4 nm for 1 at % for $T_s = 250\,°C$), then reducing to a minimum when the dopant concentration reached 12 at % (10.2 nm for $T_s = $ RT, and 8.7 nm for $T_s = 250\,°C$). It is noticed that for 1 and 2 at % the crystallite size increased with respect to that of undoped ZnO. The evolution of the ZnO lattice parameters a and c are shown in Fig. 1(c) as a function of the dopant concentration for $T_s = $ RT and $250\,°C$. The ZnO single-crystal reference values for a and c are indicated in the figure with horizontal dashed lines [3]. It is clear that the incorporation of copper and tellurium produced a unit-cell enlargement since both axes are bigger than those of the single crystal. The coordination of Zn and O in the ZnO lattice is 4 (each Zn and

O is surrounded by four nearest neighbors of different kinds in a tetrahedral arrangement). For this coordination number, the ionic radii of Cu^{2+} and Zn^{2+} are very similar: 71 and 74 pm, respectively. It is mentioned as well that the ionic radius of Cu^{1+} is 74 pm, coincidental with that of Zn^{2+}. The ionic radius of O^{2-} is 124 pm, while that of Te^{2-} may be considered close to 200 pm. (The ionic radius of Te^{2-} coordination 4 is unknown; however, it is reasonable to assume a value slightly smaller than that of Te^{2-} coordination 6, which is 207 pm, in analogy to O^{2-} whose ionic radii for coordination 4 and 6 are 124 and 126 pm, respectively.) Thus the enlargement of the unit cell may be ascribed to tellurium atoms, either when entering substitutionally (Te_O) or interstitially (Te_i). The effect of higher substrate temperatures, Fig. 1(c), is to bring the lattice parameters closer to those of the single crystal. In other words, the larger the thermal energy provided during film growth, the better the mobility of the atoms to position themselves at sites that reduce the overall lattice energy through lowering the defect-related stress energy.

Figure 2 shows 50 000x SEM images of the surfaces of the films deposited at $250\,°C$ for 1, 2, 3, 5, 7, and 12 at % of 2Cu:Te. The insets show the appearance to the eye of each film under white-light illumination. There is a correspondence between the size of the aggregates and the crystallite sizes in Fig. 1(b). In general, the films are dense with homogeneous grain sizes.

In Fig. 3 is presented the effect on the crystalline structure of varying the substrate temperature for a fixed impurity concentration (3 at %). Higher substrate temperatures brought the interplanar spacings closer to the single-crystal values (dashed vertical lines). In the case of undoped films, $350\,°C$ sufficed to obtain interplanar distances coincidental with those of the single crystal. That is, lattice defects and strain were reduced sufficiently to the point of obtaining such interplanar spacings. This did not occur, however, for the doped films because of the built-in strain in the host caused by the different ionic radii of copper and, mainly, tellurium.
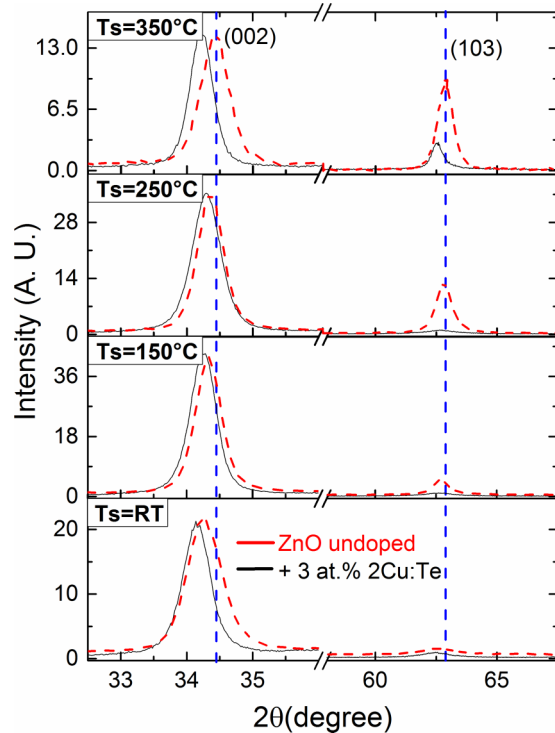
FIG. 3. Diffraction patterns of undoped ZnO films (red dashed lines) and films with 3 at % 2Cu:Te (dark gray continuous lines) for the indicated substrate temperatures. The vertical dashed lines correspond to the position of the diffraction peaks in the ZnO powder diffraction data file (PDF no. 05-0664).

B. Composition

The chemical composition of the films was determined by wavelength-dispersive spectroscopy. The measurements were carried out on films grown on pieces of silicon wafers that were placed next to the glass substrates for each run. From Fig. 4 it is noticed that the concentration of zinc and oxygen reduced in a similar manner as the dopant concentration was augmented. The only exception to this occurred when $T_s =$ 350 °C, since this temperature was appropriate to maintain the concentration of oxygen close to 50 at %, while that of zinc dropped to $\sim$32 at % for the largest dopant concentration (12 at %). Even though copper and tellurium were in a 2:1 ratio in the target, their actual concentration for most films was around 1:1, Fig. 4. The reason for this behavior is not clear at this point and will be the subject of further investigation.

C. Optical properties

The optical properties of the ZnO films were significantly modified by the presence of Cu and Te. The transmittance changed from full transparency in the visible to complete opacity. This variation could be controlled by the doping level and substrate temperature, as it may be observed in Fig. 5. Some general trends can be noticed in the optical behavior of the films. As expected, undoped films are transparent due to the large band gap of ZnO (3.3 eV), while for doped films, only the sample grown at RT with 1 at % stays transparent. As the doping level increased, the films became less transparent until becoming completely dark, especially those with 12

at %. When $T_s = 350$ °C, however, this trend was reversed so that the films recovered some transparency regardless of the doping level. The relevant parameters for the optical behavior of the films are the [Zn]/[O] ratio and the temperature during growth, as discussed next.

A striking difference is noticeable in the optical properties of the films with 7 at % grown at 250 °C and 350 °C (pictures with yellow and red cactuses in Fig. 5, respectively). To the eye, the former looks totally dark, while the latter looks translucent. The reason for this behavior cannot be accounted for by the dopant contents, since the 350 °C film has larger concentration of Cu and Te, Figs. 4(c) and 4(d), nor by the difference in oxygen concentration between the two samples, which is only $\sim$3% (250 °C film: 44 at %; 350 °C film: 47 at %). On the other hand, if attention is paid to the [Zn]/[O] ratio, the 250 °C film is 5% oxygen deficient ([O]/[Zn] = $44/46 = 0.95$), while the 350 °C film is 23% oxygen rich ([O]/[Zn] = $47/38 = 1.23$). In other words, in the 350 °C film each Zn atom has no difficulty in having available four O nearest neighbors, as in stoichiometric ZnO, plus some extra O atoms ($\sim$23 at %) to yield oxygen-rich ZnO. This is in agreement with reports where the transparency of oxygen-rich ZnO is enhanced with respect to pristine ZnO [12]. Other samples where [O]/[Zn]>1 was the batch deposited at $T_s =$ RT, Fig. 4(a), which presented a dark appearance for dopants concentration above 2 at %. In this case the film's opacity can be due to photon absorption involving defect-related electronic levels within the band gap that form after the low deposition temperature. From this analysis it may be stated that in order to obtain translucent ZnO:(Cu+Te) films, high substrate temperatures are necessary ($\gtrsim$350 °C) for producing appropriate [O]/[Zn] ratios ($\gtrsim$1.2) and for reducing defect-related absorption processes.

Spectroscopic data on the ZnO:(Cu+Te) films were obtained from UV-vis near-IR transmittance and absorbance measurements. Figure 6 shows the normal incidence transmittance spectra of undoped and doped films grown at (a) RT, (b) 250 °C, and (c) 350 °C on glass substrates. The vertical dashed line corresponds to the band-gap energy of ZnO (3.3 eV). The oscillations in the spectra are due to interference effects produced by the multiple reflections at the air/film and film/substrate interfaces. Direct-band-gap semiconductors, such as ZnO, present abrupt transmittance and absorbance edges. The edge sharpness in the transmittance spectra can be significantly reduced if the material has a large density of defects, which in turn create electronic levels within the band gap, making photon absorption possible for energies lower than E_g. This is the effect observed in Figs. 6(a) ($T_s =$ RT) and 6(b) ($T_s = 250$ °C). The larger the dopant concentration, the lower the slope of the transmittance edge. This change is indicated by the red dashed lines in the bottom and top spectra in Fig. 6(a) ($T_s =$ RT). The x-ray diffraction pattern of the film deposited at 250 °C doped with 12 at % shows that the crystalline structure of this film has been severely affected by the dopant incorporation, top pattern Fig. 1(a). The transmittance spectrum of this sample reflects the effect of such disorder: its maximum transmittance is $\sim$18%, top panel Fig. 6(b). The behavior of the transmittance for the films grown at $T_s = 350$ °C was the opposite. The edge was tilted the most for samples with the lowest dopant
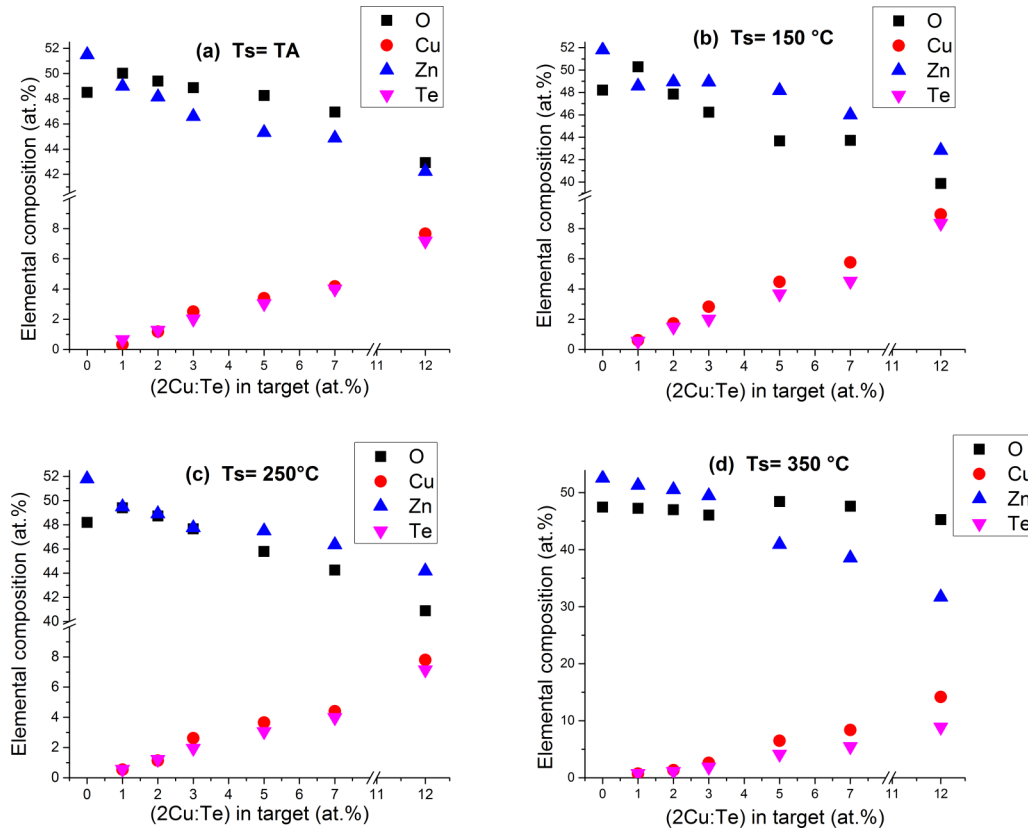
FIG. 4. Elemental chemical composition of the films determined by wavelength-dispersive spectroscopy as a function of the atomic concentration of 2Cu:Te in the sputtering target. Data are shown for films grown at (a) room temperature, (b) 150 °C, (c) 250 °C, and (d) 350 °C.

concentration, while it was the sharpest for the most doped film [top spectrum, Fig. 6(c)]. In fact, with exemption of the RT-1 at % sample [bottom panel, Fig. 6(a)], the transmittance edge of the 350 °C-12 at % film was the steepest. The high substrate temperature produced two effects: maintain

the oxygen concentration at values around 48 at %, regardless of the doping level [Fig. 4(d)], and reduce significantly the below-band-gap absorption caused by the defect-related electronic levels. Another feature worth noticing in Fig. 6 is the redshift of the absorption onset as the dual doping
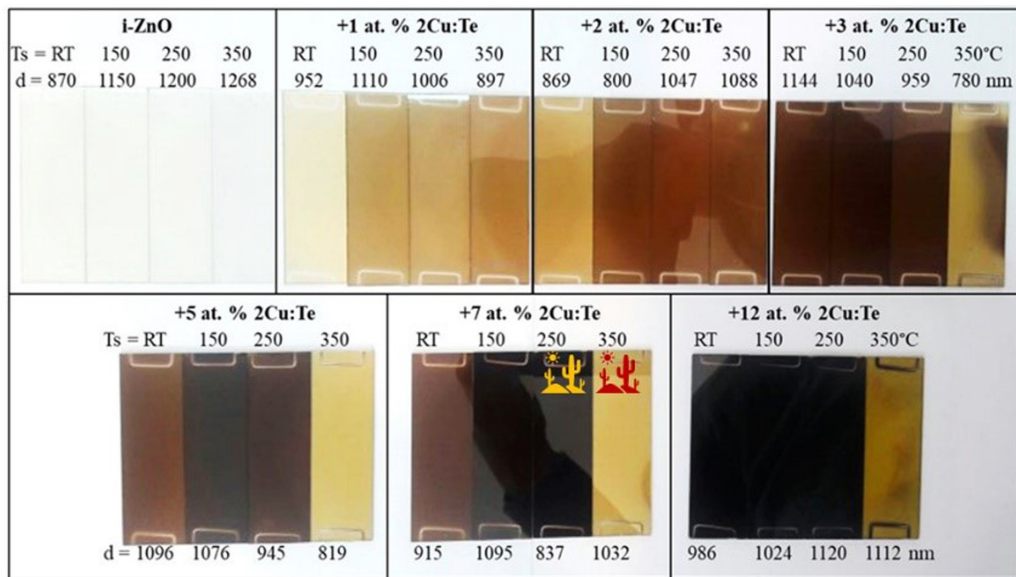

FIG. 5. Photographs of undoped and codoped films. The dopant atomic percentage, substrate temperature (T_s), and thickness in nanometers (d) for each film are indicated. The photographer and the camera can be observed in the specular reflection.
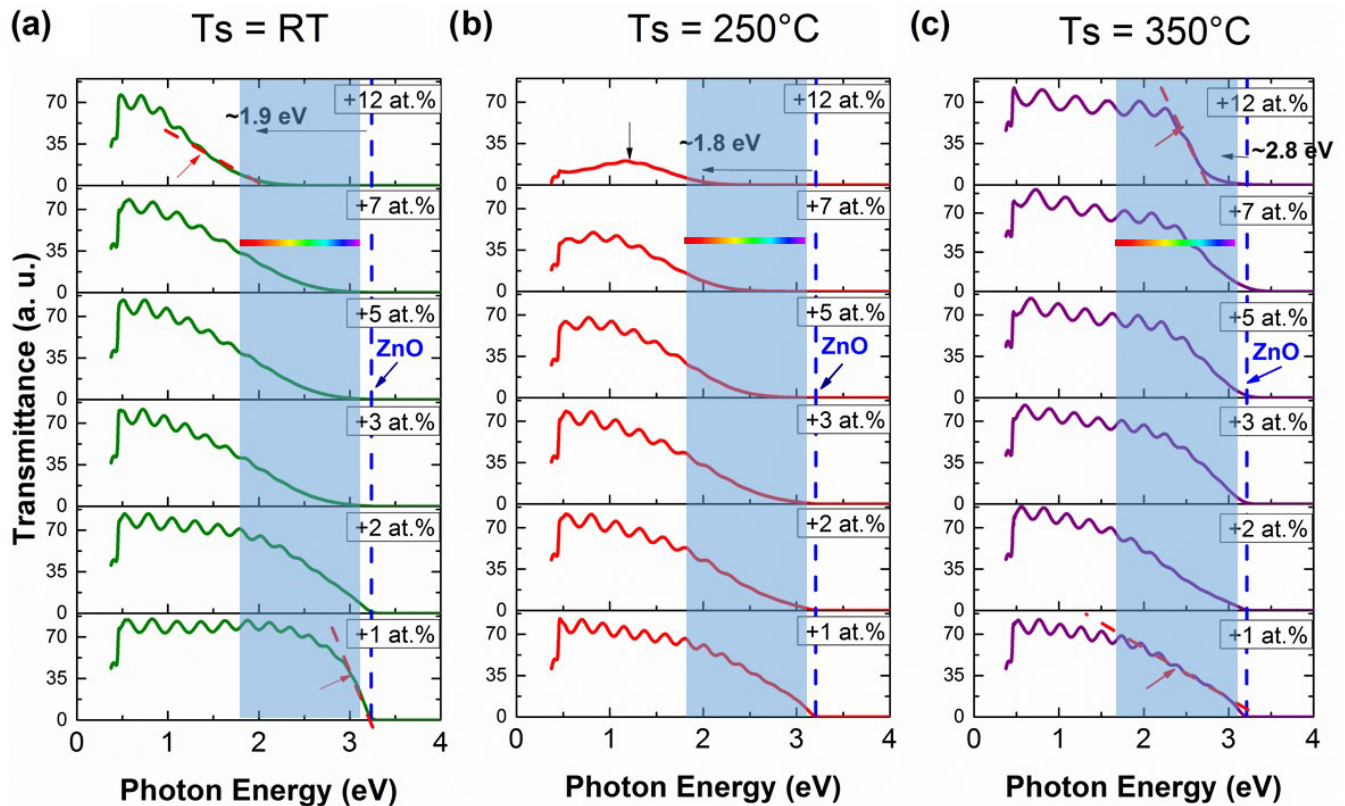
FIG. 6. Transmittance spectra of the ZnO:(Cu+Te) films grown at (a) RT, (b) 250 °C, and (c) 350 °C. The blue shaded areas depict the visible spectral region; the vertical dashed lines correspond to the band gap of undoped ZnO film. The black horizontal arrows in the top panels indicate the shift of the transmittance edge (with respect to ZnO) for the 12 at %-doped samples.

increased. In the films doped with 1 at % the onset was basically the same than for undoped ZnO, $\sim$3.2 eV, while when the doping concentration reached 12 at %, the onset was at $\sim$2.8, 1.8, and 1.9 eV for $T_s = 350$, 250 °C, and RT, respectively (top panels Fig. 6). That is, a significant band-gap renormalization occurred as a consequence of the Cu and Te codoping.

The values of the band gap were obtained through the model for direct transitions between parabolic bands described by the relation $(\alpha h\nu)^2 = B(h\nu - E_g)$, where α is the optical absorption coefficient, B is a constant, h is Planck´s constant, and ν is the frequency of the incident light. The absorption coefficient was obtained from the absorbance (A) measurements (not shown) using the relation $\alpha(\lambda) = 2.303(A/d)$, where d is the film thickness. Figure 7 shows the values of E_g for the films grown at RT and 250 °C. When $T_s = $ RT, Fig. 7(a), the band gap renormalized from 3.2 eV for undoped ZnO to 1.92 eV ($\Delta E_g = 1.28$ eV) for the film with 12 at % 2Cu:Te. Similar results were obtained for the films deposited at 250 °C, Fig. 7(b), with a minimum of 1.82 eV ($\Delta E_g = 1.38$ eV) for the most doped sample. In Fig. 7 it is shown graphically that the band gap of all doped films lies in the visible region of the spectrum.

D. Electrical properties

Dual doping with copper and tellurium produced a transition from *n*- to *p*-type conductivity in ZnO. Figure 8

shows the resistivity, mobility, and free-carrier density of the films grown at 250 °C, the batch where reliable Ohmic contacts could be obtained. The measured electrical parameters of the undoped (*n*-type) ZnO film were $\rho = 1\,\Omega$ cm, $\mu = 3.5$ cm^2/V s, and $n = 3 \times 10^{18}$ cm^{-3}. It is pointed out that when the dopant concentration was 1 at %, the films were highly resistive. Since the film with 2 at % presented *p*-type conductivity, it is reasonable to assume that the sample with 1 at % Cu:Te was highly resistive due to compensation effects. A competition exists between defects producing donorlike (natural of ZnO) and acceptorlike behavior. The results presented here substantiate that Cu+Te doping creates acceptorlike defects/complexes that oppose the native *n*-type defects/complexes. That is, above a threshold Cu+Te concentration (≈ 2 at %), acceptorlike defects/complexes prevail. Table I shows possible point defects in the films produced by the presence of Cu and Te dopants in the ZnO lattice, as well as their expected effect on the electrical performance by considering only the local charge tradeoff. The analysis included substitutional and interstitial Cu and Te, as well as native ZnO defects such as oxygen vacancies and zinc interstitials. It is well established that Cu is an acceptor impurity in ZnO, consistent with an effective substitutional charged state Cu_{Zn}^{1+}. At interstitial sites Te would act as acceptor impurity. Even though Te is isoelectronic with O, substitutional Te behaves as a light *n*-type impurity in ZnO, since its lower electronegativity produces a lower attraction for electrons than oxygen (i.e., the probability that electrons escape from a Zn-Te bond
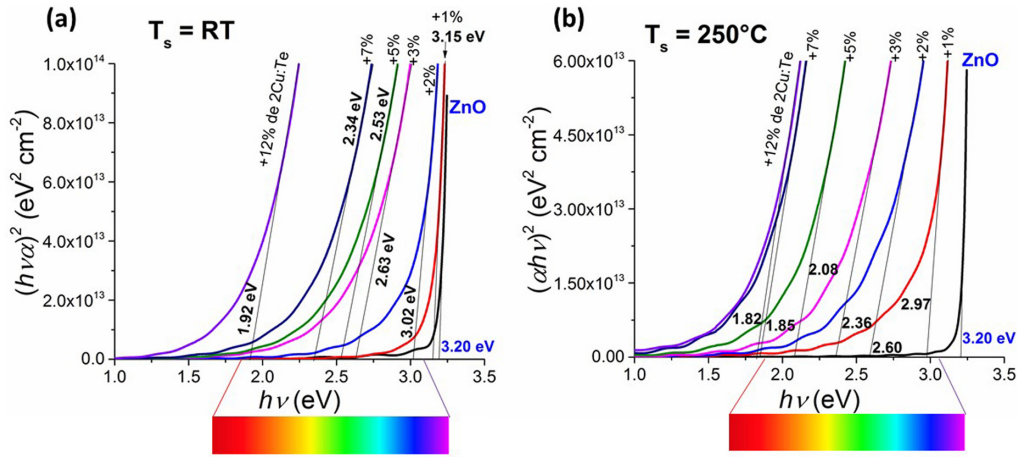
FIG. 7. Plots of $(ah\nu)^2$ vs energy ($h\nu$) for the films grown at (a) room temperature and (b) 250 °C showing the band-gap renormalization of the ZnO:(Cu+Te) films. The intersection of the extrapolated lines with the energy axis correspond to the value of the band gap for each film according to the model of direct transitions between parabolic bands. It is noticed that all values of E_g for the codoped samples lay within the visible region of the spectrum.

is larger than that from a Zn-O bond). Any combination of Te_O with well-defined *p*-type dopants (e.g., complexes such as Cu_{Zn}-Te_O and Te_i-Te_O) will result in a net *p*-type characteristic. Although x-ray diffraction did not detect $Cu_{2-x}Te$ clusters in the films, it is worth commenting on the possible presence of amorphous or nanocrystalline $Cu_{2-x}Te$, a *p*-type semimetal [13,14]. It has been reported that $Cu_{2-x}Te$ aggregates, found in CdTe:(Cu+O), for instance, arise from the strong trend between Cu and Te to form bonds that eventually evolve to $Cu_{2-x}Te$ micro- or nanoclusters [15–17]. It has been shown that the existence of amorphous or nanocrystalline copper telluride (not detected through x-ray diffraction) can be evidenced through optical transmission experiments in which a characteristic bell-shaped low-intensity band centered around 900 nm is observed [17]. This feature is not present in any of the transmission spectra of the ZnO:(Cu+Te) films, which strongly suggests that copper telluride does not form to any significant extent in the samples.

The evolution of the free-hole density as a function of dopant content (see inset Fig. 8) evidences a continuous transformation from *n*- to *p*-type conductivity. The free-electron

density for the undoped *n*-type ZnO film was of the order of 10^{18} cm^{-3}. Then at 1 at % doping the sample became highly resistive, as strong compensation effects took place. The films were conducting again after raising the dopant concentration to 2 at %; however, the free-carrier density dropped four orders of magnitude (to 10^{14} cm^{-3}). As the dopant concentration rose, the free-hole density increased smoothly until densities of the order of 10^{20} cm^{-3} were attained for concentrations of 5 at % and above. Overall, the resistivity of the films changed from 2×10^3 (2 at %) to 6×10^{-2} Ω cm (12 at %), a five orders of magnitude reduction. Regarding mobility, it was 4 cm^2/V s for the 2 at % sample, slightly higher than that of undoped ZnO. However, the mobility dropped to values $\sim$0.01 cm^2/V s for films doped with 3 and 5 at %. Upon additional doping, however, it increased two orders of magnitude when the dopant concentration was 12 at %, reaching $\sim$1 cm^2/V s. The mobility improved one-and-a-half orders with respect to its lowest value for the most doped films. In general, when the long-range periodicity of the crystalline structure is affected by defects, the carrier mobility is reduced, since defects act as scattering centers. The x-ray

TABLE I. Defects in the ZnO:(Cu+Te) films and their expected effect on the charge transport properties. The Kröger-Vink notation for defects in crystals has been employed (middle column), which considers effective charges (the charge that the defect has with respect to the charge that would be present at the same site in a perfect crystal). The expected effect on the electrical properties (last column) describes the charge tradeoff around the indicated defect; it does not take into consideration the actual Fermi-level position, ionization energies, or complex formation, which may modify the behavior annotated in the column [18].

| Dopant	Status in ZnO lattice	Expected effect on the electrical properties
Cu	Substitutional, Cu_{Zn}	Cu^{1+}, *p*-type dopant
	interstitial, $Cu_i^{2\bullet}$	Cu_i^{2+}, *n*-type dopant
Te	Substitutional (isoelectronic), Te_O	Te (isoelectronic with O) has electronegativity lower than O, light *n*-type dopant
Te	Interstitial, $Te_i^{2'}$	Te^{1-}, Te^{2-}, if 1 or 2e^- are trapped, respectively, *p*-type dopant
O, native	Oxygen vacancy, $V_O^{2\bullet}$	*n*-type dopant
Zn, native	Interstitial, $Zn_i^{2\bullet}$	Zn_i^{2+}, *n*-type dopant
Zn, native	Zinc vacancy, $V_{Zn}^{2'}$	*p*-type dopant
Cu, Te	Cu_{Zn} + $Te_i^{2'}$	*p*-type dopant
Cu, Te	Cu_{Zn} + Te_O	*p*-type dopant
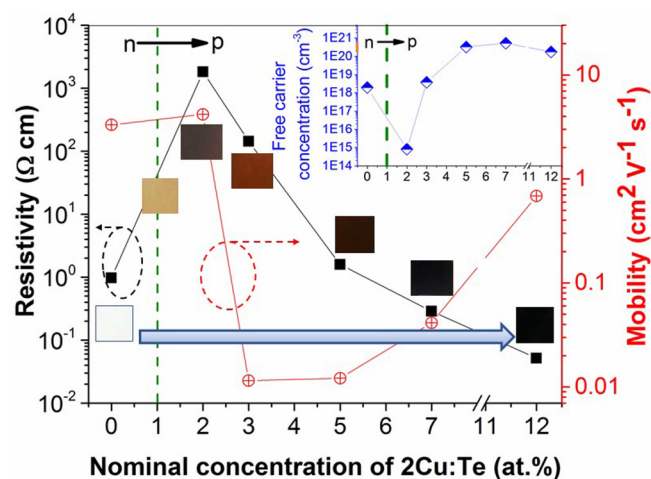
FIG. 8. Resistivity, mobility, and free-carrier concentration of undoped and ZnO:(Cu+Te) films deposited at $T_s = 250\,°C$ as a function of the dopant nominal concentration in the target. Data for [2Cu:Te] = 1 at % could not be obtained because the sample was highly resistive due to compensation effects. Next to the data points for each concentration appears a section of the corresponding photograph in Fig. 5. The thick horizontal arrow highlights the evolution from full transparency to complete opacity in the visible when going from undoped to 12 at % films.

diffraction pattern of the 12 at %-250 °C sample (top panel, Fig. 1) shows that high doping significantly affected the crystalline structure. Thus it would be expected that the mobility of this sample was near that of an amorphous material (typically between 10^{-2} and $10^{-1}\,cm^2/V\,s$), given

its structural characteristics. Nonetheless, the mobility of this sample was larger than that of the less-doped films whose crystallinity was less compromised. To address this matter, two possible mechanisms may be considered: (i) Given the large size of the Te impurities (the radius of Te^{2-} is 61% larger than that of O^{2-} and 270% larger than Zn^{2+}), interstitial and/or substitutional Te atoms may effectively act as bridges at interstitial sites and/or fill oxygen vacancies, aiding the charge transport and, thus, the overall conductivity. This possible mechanism is illustrated in Fig. 9. Under this scheme, two competing mechanisms could be in effect: the detrimental for mobility *scattering center effect*, and the beneficial for mobility *bridging effect*. According to the mobility data in Fig. 8, for samples with dopant concentrations of 3 and 5 at %, scattering from ionized impurities would be the dominant process affecting the mobility; for 7 at % the bridging effect would start taking over, becoming clearly dominant when [2Cu:Te] reaches 12 at %. Such a bridging effect would be similar to a percolation mechanism in the sense that alternative paths for free-carrier transport were established by the large-size Te atoms. The mobility data, nevertheless, does not present the characteristic abrupt change observed when the percolation threshold is reached, not to mention the fact that the impurity concentrations used here are far lower than the cation percolation threshold (19.8%) for wurtzite ZnO [19]. (ii) Previous findings in ZnO films indicate that growth defects constitute preferred sites for impurities [20]. The grain size data of the films grown at $T_s = 250\,°C$, Fig. 1(b), show that the smallest crystallite size (8.7 nm) corresponds to the sample doped with 12 at %. Since the most doped sample simultaneously has the lowest resistivity and
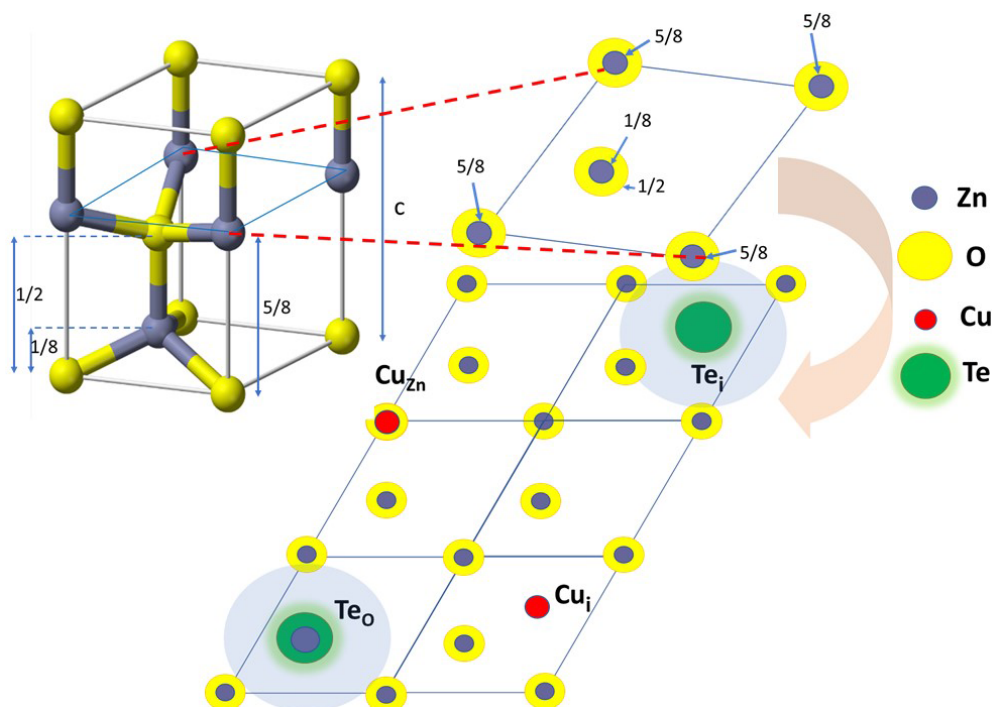

FIG. 9. (top) ZnO hexagonal unit cell depicting a projection to the basal plane (top right) of the atoms whose *c*-axis fractional coordinates are indicated. (bottom) Two-dimensional projection of the ZnO structure describing randomly located Cu_{Zn}, Cu_i, Te_O, and Te_i impurities. Cu_{Zn} Te_i and the complexes $Cu_{Zn} + Te_i$ and $Cu_{Zn} + Te_O$ may act as acceptors.

TABLE II. Electrical parameters for films grown at the indicated substrate temperature (T_s) and dopant concentrations in the sputtering target.

T_s [°C]	2Cu:Te in target [at %]	Resistivity [Ω cm]	Mobility [cm^2/V s]	Free-carrier density [cm^{-3}]	Conductivity type
RT	Undoped ZnO	3.3×10^{-3}	54.5	3.5×10^{19}	*n*
150	Undoped ZnO	1.5×10^{-2}	37.9	1.1×10^{19}	*n*
150	5	48.33	0.19	6.9×10^{17}	*n*
150	7	2.12	2.25	1.3×10^{18}	*n*
150	12	1.41	0.018	2.5×10^{20}	*p*
RT	12	62.70	0.074	1.4×10^{18}	*p*
350	2	42.56	0.018	8.1×10^{17}	*p*

the smallest grain size, it is reasonable to hypothesize that a fraction of the Cu+Te dopants participate in grain boundary passivation to the extent of effectively assisting intergrain and interdefect carrier transport. The rest of the dopants would play an important role in enhancing conductivity within the crystallite volume.

In addition to the series grown at 250 °C, the electrical properties of samples grown at other temperatures, to which reliable Ohmic contacts were possible, are presented in Table II. From these data, two conclusions can be drawn as to the appropriate conditions for producing the transition from *n*-type conductivity to *p*-type: high substrate temperatures and/or large Cu+Te concentrations. An example of the former is the 2 at % film deposited at 350 °C; an example of the latter is the 12 at % film grown at RT. It is noticed that a substrate temperature of 150 °C was not enough to generate *p*-type films when the targets had dopant concentrations of 5 and 7 at %. For that temperature, it took 12 at % of 2Cu:Te in the target to transform ZnO:(Cu+Te) into a *p*-type material.

Tellurium has been used in the past as codopant in ZnO to investigate its effects on the properties of *N*-doped ZnO. Porter *et al.* prepared films of ZnO:(N+Te) by pulsed laser deposition, finding an enhanced photoconductivity and higher resistivity as a result of the doping process [21]. Molecular beam epitaxy was employed by Park *et al.* to deposit (N+Te) codoped ZnO films, obtaining *p*-type layers with resistivities between 13 and 49 Ω cm, mobilities of 11 and 21 cm^2/V s, and free-carrier densities in the range of 10^{15}–10^{16} cm^{-3}, depending on the Te flux density during growth [22]. N+Te codoping was used to realize ZnO films grown at 400 °C by MOCVD, resulting in resistivities of the order of 10^2 Ω cm, carrier densities of $\sim 10^{16}$ cm^{-3}, and mobilities in the range of 10^{-1} cm^2/V s for as-grown films [9]. In none of these works, where Te participated as codopant, did the band gap of the ZnO host have a significant variation as occurred under Cu+Te codoping. In regard to the electrical parameters, some improvement in tailoring them was achieved by Cu+Te codoping in the sense that a wider range in resistivity and free-hole density were attained with respect to previous works.

II. CONCLUSIONS

The conductivity of ZnO films was successfully transformed from *n*- to *p*-type through an alternative dual doping approach where copper and tellurium were incorporated in the ZnO lattice. The dopants were used in appropriate amounts to yield atomic concentrations between 1% and 12%. The transformation was successful for high sub-

strate temperatures (e.g., 350 °C, 2 at %) and/or large dopant content (e.g., RT, 12 at %). For films deposited at 250 °C, it was possible to make a full characterization. Specifically, reliable Ohmic contacts were attainable for this batch, in which it was possible to control the resistivity (10^3–10^{-2} Ω cm), mobility ($\sim 10^{-2}$–10^0 cm^2/V s), and free-hole density (10^{15}–10^{20} cm^{-3}) by changing the Cu+Te concentration. These changes were accompanied by a gradual band-gap renormalization that moved the absorption edge from the UV (3.2 eV) to the red (1.8 eV). In other words, codoping with Cu and Te modified the ZnO band structure so that the films were increasingly more absorbent in the visible as the concentration of Cu+Te rose. This loss of transparency, although inconvenient for applications in transparent electronics, is advantageous for devices based on photonic absorption/emission. In fact, this property opens the possibility for fabrication of all-ZnO homojunctions of the type *n*-ZnO/*p*-ZnO:(Cu+Te), amenable for optoelectronic devices such as light-emitting diodes and solar cells [23,24].

III. EXPERIMENTAL

Thin films of undoped ZnO and ZnO:(Cu+Te) were deposited on glass substrates and on *n*-type Si wafers by magnetron sputtering. The chemical composition was obtained from the films deposited on Si to avoid misleading oxygen signals if glass substrates were employed for this purpose. Prior to growth, the glass substrates and silicon wafers were cleaned through standard procedures. A target of two inches in diameter was prepared by cold pressing a mixture of ZnO (99.99%), Cu (99.5%), and Te (99.997%) powders. Targets were prepared of undoped ZnO and of ZnO:(Cu+Te) with 1, 2, 3, 5, 7, and 12 at % nominal concentrations of Cu:Te, in an atomic ratio of 2:1. That is, 1% of (2Cu:Te) means that the target had 99.00 at % ZnO, plus 0.66 at % Cu, and 0.33 at % Te, with a similar meaning for the other concentrations. Other growth parameters were Ar flow rate = 11 sccm, working pressure = $\sim$0.3 Pa, rf power = 100 W, target-to-substrate distance = 8 cm, presputtering time = 5 min, and deposition time = 90 min. The substrate temperature for different runs was room temperature, 150 °C, 250 °C, and 350 °C.

The chemical composition of the samples was determined by wavelength-dispersive spectroscopy (WDS) in a Phillips ESEM scanning electron microscope XL30. The same instrument was used to characterize the surface morphology. The structural analysis was performed by x-ray diffraction (XRD, D/Max-2100, Rigaku) using Cu Kα radiation (λ = 1.5406 Å). The optical transmittance and reflectance at normal incidence

were measured in a UV-vis NIR spectrophotometer (Film Tek 3000) equipped with a deuterium-halogen lamp. The electrical properties of the films were investigated in a Hall-effect measurement system (Ecopia HMS-3000) using the van der Pauw configuration.

The data that support the findings of this study are available from the corresponding author upon reasonable request.

1. J. Theerthagiri1, S. Salla, R. A. Senthil, P. Nithyadharseni, A. Madankumar, P. Arunachalam, T. Maiyalagan, and H. S. Kim, A review on ZnO nanostructured materials: Energy, environmental and biological applications, Nanotechnology **30**, 392001 (2019).

2. J. Wang, R. Chen, L. Xiang, and S. Komarneni, Synthesis, properties and applications of ZnO nanomaterials with oxygen vacancies: A review, Ceram. Int. **44**, 7357 (2018).

3. H. Morkoç and Ü. Özgür, *Zinc Oxide: Fundamentals, Materials and Device Technology* (Wiley-VCH Verlag GmbH, Weinheim, Germany, 2009), pp. 246–264.

4. Ü. Ozgur, Ya. I. Alivov, C. Liu, A. Teke, M. A. Reschikov, S. Doğan, V. Avrutin, S.-J. Cho, and H. Morkoç, A comprehensive review of ZnO materials and devices, J. Appl. Phys. **98**, 041301 (2005).

5. Y. F. Yan, Y. Li, S. H. Wei, and M. M. Al-Jassim, Possible Approach to Overcome the Doping Asymmetry in Wideband Gap Semiconductors, Phys. Rev. Lett. **98**, 135506 (2007).

6. M. A. Borysiewicz, ZnO as a functional material, a review, Crystals **9**, 505 (2019).

7. Z. Ma, F. Ren, X. Ming, Y. Long, and A. A. Volinsky, Cu-doped ZnO electronic structure and optical properties studied by first-principles calculations and experiments, Materials **12**, 196 (2019).

8. K. Tang, S. L. Gu, J. D. Ye, S. M. Zhu, R. Z. Zhang, and Y. D. Zheng, Recent progress of the native defects and *p*-type doping of zinc oxide, Chin. Phys. B **26**, 047702 (2017).

9. K. Tang, S. Gu, K. Wu, S. Zhu, J. Ye, R. Zhang, and Y. Zheng, Tellurium assisted realization of *p*-type *N*-doped ZnO, Appl. Phys. Lett. **96**, 242101 (2010).

10. S. Sönmezoglu and E. Akman, Improvement of physical properties of ZnO thin films by tellurium doping, Appl. Surf. Sci. **318**, 319 (2014).

11. F. Khosravi-Nejada, M. Teimourib, S. J. Marandia, and M. Shariati, The highly crystalline tellurium doped ZnO nanowires photodetector, J. Cryst. Growth **522**, 214 (2019).

12. X. Yao, J. Liang, T. Li, L. Fan, B. Shi, C. Wei, Y. Ding, Y. Li, Y. Zhao, and X. Zhang, Electron transport layer driven to improve the open-circuit voltage of CH$_3$NH$_3$PbI$_3$ planar perovskite solar cells, Sci. China Mater. **61**, 65 (2018).

13. A. H. Barajas-Aguilar, S. Jiménez-Sandoval, and A. M. Garay-Tapia, On the stability of Cu$_x$Te polytypes: Phase transitions, vibrational and electronic properties, J. Phys.: Condens. Matter **32**, 045403 (2020).

14. J. U. Salmón-Gamboa, A. H. Barajas-Aguilar, L. I. Ruiz-Ortega, A. M. Garay-Tapia, and S. Jiménez-Sandoval, Vibrational and electrical properties of Cu$_{2-x}$Te films: Experimental data and first principle calculations, Sci. Rep. **8**, 8093 (2018).

15. A. Mendoza-Galván, G. Arreola-Jardón, L. H. Karlsson, P. O. Å. Persson, and S. Jiménez-Sandoval, Optical properties of CuCd-TeO thin films sputtered from CdTe-CuO composite targets, Thin Solid Films **571**, 706 (2014).

16. G. Arreola-Jardón, S. Jiménez-Sandoval, and A. Mendoza-Galván, Growth and characterization of CuCdTeO thin films sputtered from CdTe-CuO composite targets, Vacuum **101**, 130 (2014).

17. J. Carmona-Rodríguez, R. Lozada-Morales, P. del Angel-Vicente, O. Jiménez- Sandoval, G. López-Calzada, D. Dahlberg, and S. Jiménez-Sandoval, Properties of Cu$_x$(CdTe)$_y$O$_z$ thin films: Composition-dependent control of band gap and charge transport, J. Mater. Chem. **21**, 13001 (2011).

18. A. Janotti and C. G. Van de Walle, Fundamentals of zinc oxide as a semiconductor, Rep. Prog. Phys. **72**, 126501 (2009).

19. N. Ali, B. Singh, Z. A. Khan, A. R. Vijaya, K. Tarafder, and S. Ghosh, Origin of ferromagnetism in Cu-doped ZnO, Sci. Rep. **9**, 2461 (2019).

20. A. Dadgar, A. Krtschil, F. Bertram, S. Giemsch, T. Hempel, P. Veit, A. Diez, N. Oleynik, R. Clos, J. Christen, and A. Krost, ZnO MOVPE growth: From local impurity incorporation towards *p*-type doping, Superlattice Microstruct. **38**, 245 (2005).

21. H. L. Porter, A. L. Cai, J. F. Muth, and J. Narayan, Enhanced photoconductivity of ZnO films Co-doped with nitrogen and tellurium, Appl. Phys. Lett. **86**, 211918 (2005).

22. S. Park, T. Minegishi, D. Oh, H. Lee, T. Taishi, J. Park, M. Jung, J. Chang, I. Im, J. Ha, S. Hong, I. Yonenaga, T. Chikyow, and T. Yao, High-quality *p*-type ZnO films grown by Co-doping of N and Te on Zn-face ZnO substrates, Appl. Phys. Express **3**, 031103 (2010).

23. M. Su, T. Zhang, J. Su, Z. Wang, Y. Hu, Y. Gao, H. Gu, and X. Zhang, Homogeneous ZnO nanowire arrays p-n junction for blue light-emitting diode applications, Opt. Express **27**, A1207 (2019).

24. A. Saboor, S. M. Shah, and H. Hussain, Band gap tuning and applications of ZnO nanorods in hybrid solar cell: Ag-doped versus Nd-doped ZnO nanorods, Mater. Sci. Semicond. Process. **93**, 215 (2019).